

Ab initio calculations of the B1-B2 phase transition in MgOJ. Bouchet,¹ F. Bottin,¹ V. Recoules,¹ F. Remus,¹ G. Morard,² R. M. Bolis,^{3,4} and A. Benuzzi-Mounaix^{3,4}¹CEA, DAM, DIF, F-91297 Arpajon, France²Sorbonne Université, Institut de Minéralogie, de Physique des Matériaux et de Cosmochimie, IMPMC, Museum National d'Histoire Naturelle, UMR CNRS 7590, Paris, France³LULI-CNRS, Ecole Polytechnique, CEA, Université Paris-Saclay, Palaiseau cedex, F-91128, France⁴Sorbonne Université, UPMC Univ Paris 06, CNRS, Laboratoire d'utilisation des lasers intenses (LULI), place Jussieu, Paris cedex 05, 75252, France

(Received 26 October 2018; published 29 March 2019)

We present an *ab initio* study of MgO at high temperature and pressure, around the phase transition between the B1 and B2 phases. By means of *ab initio* molecular dynamic calculations, the thermal evolution of vibrational properties and thermodynamic quantities is obtained. We carefully compare our results with previous theoretical works on the phase transition curve and we analyze the differences among them. We show that anharmonic effects have been underestimated in the quasiharmonic approximation and that their inclusion in the free energy strongly straightens up the transition curve. Then, we use our B1-B2 phase boundary and our calculated Hugoniot to analyze recent decaying shock experiments on MgO. We also provide important thermodynamic quantities as the Grüneisen parameter and sound velocities and we discussed their temperature dependence.

DOI: [10.1103/PhysRevB.99.094113](https://doi.org/10.1103/PhysRevB.99.094113)**I. INTRODUCTION**

As one of the major components of the Earth's lower mantle, MgO has been extensively studied experimentally and theoretically. Since the NaCl (B1) structure is stable up to several megabars and 1000° K, MgO is also considered as an internal pressure standard and considerable efforts have been made to build its *P-V-T* equation of state (EOS). With the discovery of super-Earths, it is also crucial to extend the thermodynamic data of MgO up to pressures and temperatures expected in these massive exoplanets [1], but also for the rocky core of gas and ice giants [2,3]. It has been theoretically predicted for a long time that MgO undergoes a phase transition between the rocksalt structure to the caesium chloride (B2) structure in the 400–600 GPa range [4–12]. Experimentally, the transition has only been directly observed recently by dynamic x-ray diffraction measurements [13], and its probable signature in laser-driven decaying [14,15] and steady shock experiments [12,16] has been evidenced.

At 0 K, the more recent *ab initio* calculations are in close agreement and therefore they have a narrower range of the transition pressure between 475–510 GPa [9–12] (see Fig. 1). The small differences in the results can be incriminated to the flavor of the functional used to describe the exchange correlation term: LDA [7,9,17] or GGA (PBE [10,18], AM05 [11,12,19]). At high temperature, the disagreement on the location of the phase boundary dramatically increases, from 7% at 0 K, up to 40% at 8000 K between the lowest transition pressure (~310 GPa [12]) and the highest one (~440 GPa [10]) (see Fig. 1). One of the goals of this paper is to understand these discrepancies and to propose a well-established phase transition boundary.

All the methods used to compute the phase transition line between the B1 and B2 structures are based on a

decomposition of the Helmholtz free energy between the static part, or cold curve, obtained at 0 K and the ionic or vibrational contribution coming from the atomic motions in temperature. Since the methods are in good agreement for the transition pressure at 0 K, the differences are due to the way of obtaining the vibrational part. The key ingredient of this contribution is the phonon spectra, or rather the number of phonon states by energy, the phonon density of states (PDOS) that can be used to calculate the vibrational free energy. The phonon spectra can be obtained at 0 K using either the density functional perturbation theory [20–22] (DFPT) or the finite displacements method [23]. Based on these calculations performed at several volumes, the so-called quasiharmonic approximation [24] (QHA) introduces a temperature dependence of the phonon frequencies through thermal expansion that alters the volume of the solids. Applied to MgO [6,9], the QHA predicts the lowest phase boundary and favors the B2 phase over the B1 phase at high temperature with a close to zero Clausius-Clapeyron slope above 8000 K (see Fig. 1). Despite its usefulness and wide application, the QHA suffers from two major flaws: (i) it cannot be applied if the crystal structure is dynamically unstable at 0 K, as the bcc phase of Zr [25], Li [26], or the actinides [27,28] and (ii) it neglects the intrinsic thermal effects in opposition to the extrinsic volume dependence.

To test the robustness of the QHA, Glensk *et al.* [29] have recently studied the anharmonicity of several fcc metals using upsampled thermodynamic integration [30]. They show the importance of the anharmonic effects, even at temperatures far below the melting point. More specifically, the validity domain of the QHA for MgO has been studied by Erba *et al.* [31] and Wu *et al.* [32] by a careful comparison with experimental data for several thermodynamic quantities. At room pressure, they estimate that the QHA is valid up to about

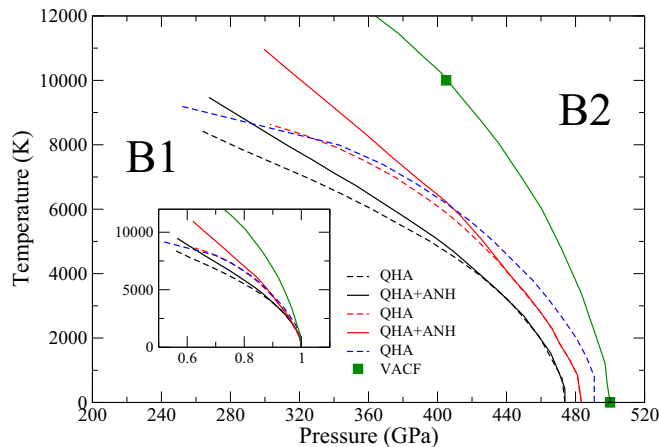


FIG. 1. Theoretical B1-B2 phase boundary of MgO. Dotted lines: quasiharmonic approximation of Root *et al.* [12] (black line), Belonoshko *et al.* [9] (blue line), and Cebulla *et al.* [11] (red line). The black and red lines include anharmonic corrections beyond the quasiharmonic approximation. The green squares are the results of Boates *et al.* [10] using velocity autocorrelation function and the green line a Kechin fit to these data. The inset shows the renormalization of the thermal transition pressures by the athermal one.

1000 K, and up to 3000 K at 100 GPa (around 30%–40% of the melting temperature). This domain of validity of the QHA has to be taken cautiously, particularly when looking at phase transitions where differences of a few meV in the Gibbs free energy can induce a difference of several GPa on the transition pressure. Basically, the QHA will fail if the phonon frequencies have a strong temperature dependence, i.e., when atomic vibrations increase in magnitude compared to the atomic distance, as for example close to the melting point but also at a phase transition where soft modes can appear.

To correct the QHA, Cebulla *et al.* [11] and Root *et al.* [12] have used *ab initio* molecular dynamics (AIMD) but their methods still rely on the QHA to deal with temperatures where anharmonicity has to be included in the estimation of the free energy. Nonetheless, their results show that the QHA overestimates the stability domain of the B2 phase in temperature and that the anharmonic effects drive to higher transition pressures at higher temperatures (see Fig. 1). Using Fourier analysis of the velocity autocorrelation function from AIMD, Boates *et al.* [10] observe a similar effect but with a stronger intensity at 10 000 K. Although this method should in principle include the whole anharmonicity present in the AIMD it requires long simulations and large supercells to avoid finite-size effects, as when employed with classical molecular dynamics. In Ref. [10], they used supercells of 64 and 128 atoms to simulate the B1 and B2 phases, rather small numbers compared to the several thousand atoms used in classical MD.

In the past 10 years, strong efforts have been made to take into account explicit temperature effects and major advances have been obtained. New methods capturing the thermal properties of solids at nonzero temperature are now available and can be applied with *ab initio* calculations. These approaches combine ideas including finite large displacements, molecular dynamics sampling, self-consistent harmonic

theories, and different force fitting schemes. The most widely used methods include self-consistent *ab initio* lattice dynamics (SCAILD) [25], stochastic self-consistent harmonic approximation (SSCHA) [33,34], temperature-dependent effective potential (TDEP) [26,35,36], anharmonic lattice model (ALAMODE) [37], compressive sensing lattice dynamics [38]. Other methods obtain anharmonic contributions via a derivation of the Gibbs energy [29] or a series expansion of the interatomic forces constants [39]. A large number of phenomena, intrinsically temperature dependent, can now be captured: the modification of the PDOS and free energy, the (T, P) phase transition boundaries, the evolution of elastic constants or Grüneisen coefficients, the phonon lifetimes, the thermal conductivity.

Here, we have used the TDEP technique developed by Hellman and co-workers [26,35,40] to extract the vibrational frequencies from AIMD simulations, with an original implementation in the ABINIT package [41,42]. This method takes roots in the pioneering work of Hooton [43] and Esfarjani *et al.* [39] and has already been successful to describe phase transitions at high temperature as for Ti and Zr [26,44], ^4He [35], or U and Pu [27,28]. In TDEP, a Taylor expansion on the atomic displacements is used to fit the Born-Oppenheimer molecular dynamics potential energy surface at finite temperature and to obtain the interatomic force constants (IFC). The second-order IFCs give the phonon frequencies while the higher-order terms can be used to calculate phonon lifetimes, thermal conductivity, or the Grüneisen parameter.

The paper is structured as follows. In Sec. II we give the details of the AIMD simulations and the construction of the free energy. In Sec. III we give our results for the B1-B2 transition curve and we compare our results with previous calculations and recent experiments. This is followed by the presentation of several thermodynamics quantities including thermoelasticity, Grüneisen parameter, and wave velocities.

II. SIMULATION DETAILS

Simulations were performed using the ABINIT package [41,42] in the framework of the projector augmented wave (PAW) method [45,46] and by means of the local density approximation (LDA) [17]. Using ATOMPAW [47–49], we generated a PAW atomic data with a radius r_{PAW} equal to 1.0 Å, with $2s$, $2p$, $3s$, and $3p$ states as valence electrons (10 electrons) for Mg and a radius r_{PAW} equal to 0.6 Å, with $2s$ and $2p$ states as valence electrons (6 electrons) for O. The cutoff energy chosen for the plane-wave set along the simulations is 816 eV. To determine the B1-B2 phase boundary, we need to calculate the free enthalpy G of both phases, with

$$G(T, P) = F(T, P) + PV(T, P), \quad (1)$$

where the free energy F is given by

$$F(T, V) = E_0(V) + F_{\text{vib}}(V, T) + F_{\text{el}}(V, T). \quad (2)$$

Here, $E_0(V)$ is the energy of the static lattice, F_{vib} the vibrational free energy due to the atomic motions, and F_{el} the electronic free energy. For the static calculations, at $T = 0$ K, we use the unit cells of the B1 and the B2 phases with two atoms and an $8 \times 8 \times 8$ Monkhorst-Pack mesh.

To obtain the vibrational part we use two methods: the QHA and the TDEP. They differ in the way of calculating the interatomic force constants (IFCs). The QHA is based on static calculations, so at 0 K, involving only the unit cells and the DFPT. The dynamical matrices are calculated on a grid of \mathbf{q} points and then Fourier transformed, yielding to the IFCs. With this method, the phonon frequencies are only dependent of the volume. Our calculations were performed on a $4 \times 4 \times 4$ grid of \mathbf{q} points in the Brillouin zone. The second method, the TDEP [26,35], calculates directly the IFC in real space from sets of forces and displacements obtained from AIMD. For this purpose, we use supercells of 128 atoms for the B1 and B2 phases, corresponding to $4 \times 4 \times 4$ rhombohedral B1 unit cells and cubic B2 unit cells (we also use larger and smaller supercells for convergence studies, see below Fig. 4). Note that contrary to previous calculations [10–12], also based on AIMD, we use the same number of atoms for the two structures. Our AIMD were performed with a $2 \times 2 \times 2$ Monkhorst-Pack mesh leading to the inclusion of four special \mathbf{k} points. This mesh was checked against a $3 \times 3 \times 3$ Monkhorst-Pack mesh to ensure the required accuracy, less than 1 meV on the vibrational free energy. Simulations were performed in the NVT ensemble (constant number of particles, constant volume, and temperature) and were run for about 5 ps using a time step (τ) of 0.60 fs. Taking into account the whole symmetries of the system, we have to calculate 19 coefficients for the B1 phase (up to the eighth shell of nearest neighbors) and 21 coefficients for the B2 phase (up to the ninth shell of nearest neighbors) to build the IFC matrices with the TDEP. So, contrary to the DFPT which uses unit cells, the TDEP requires AIMD on supercells of atoms to obtain the IFCs at a sufficiently large distance where they become negligible. It is therefore much more expensive in terms of computational time but goes beyond the QHA since the phonon frequencies are not only volume dependent, but also explicitly temperature dependent.

Once the IFC are obtained, by either method, a Fourier transform is performed to get the dynamical matrix at any \mathbf{q} point of the Brillouin zone and to calculate the PDOS. Then, the free energy is given by

$$F_{\text{vib}}(V, T) = k_B T \int_0^\infty d\omega g(\omega(V, T)) \ln \times [2 \sinh(\hbar\omega(V, T)/2k_B T)], \quad (3)$$

where the temperature dependence of the phonon frequencies ω and the PDOS $g(\omega)$ is only valid for the TDEP method. Once the free energies are calculated with Eq. (2), they are fitted by a Vinet EOS to obtain their pressure dependence and then the free enthalpy with Eq. (1).

III. B1-B2 PHASE TRANSITION

A. QHA versus TDEP method

We show in Fig. 2 the variation of the PDOS as a function of temperature obtained with TDEP for the B1 and B2 phases at a fixed density of 6.75 g/cm^3 . For both structures, the whole spectra soften with temperature. This softening is a signature of explicit thermal effects, and since in QHA the spectrum is independent of the temperature at fixed volume,

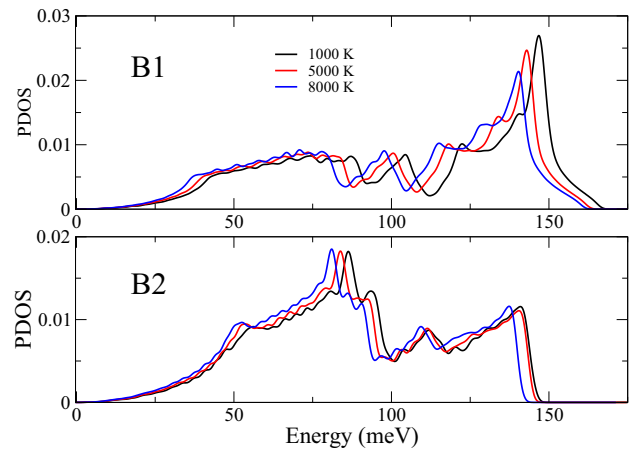


FIG. 2. PDOS of the B1 and B2 phases of MgO at 6.75 g/cm^3 and for temperatures of 1000, 5000, and 8000 K.

it will induce lower vibrational free energies in TDEP. This is directly seen in Fig. 3 where we compare the free energies obtained with both methods. Up to about 2000 K, both methods give the same free energies, but at higher temperatures the free energies obtained with TDEP deviate from the QHA. More importantly, the free-energy difference $\Delta F_{\text{vib}} = F_{\text{vib}}^{\text{B1}} - F_{\text{vib}}^{\text{B2}}$ is smaller in TDEP, as shown in the inset of Fig. 3. This means that the QHA overestimates the stability domain of the B2 phase compared to the TDEP method. In other words, the intrinsic anharmonic effects will move the phase boundary at higher pressure at high temperature, in agreement with previous works [10–12].

We have also applied the TDEP method on several supercell sizes: 64, 128, and 216 atoms for the B1 phase and 54, 128, and 250 atoms for the B2 phase. The vibrational free-energy differences between the B1 and B2 phases ΔF_{vib} are shown on Fig. 4 as a function of the supercell sizes. At 2000 K, the effect of the supercell size is negligible, and the TDEP method is close to the QHA for all the volumes considered.

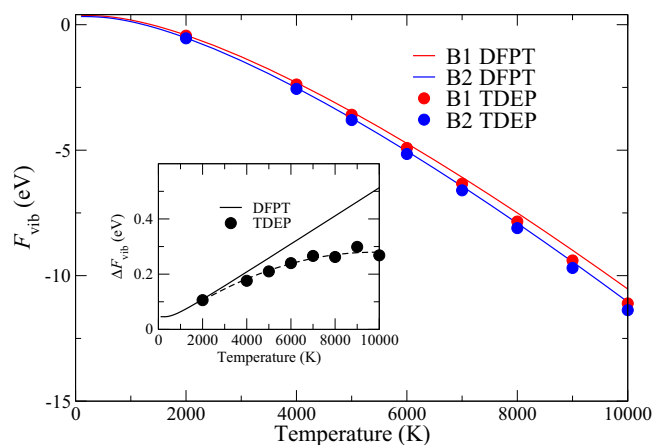


FIG. 3. Comparison of the vibrational free energies of the B1 (in red) and B2 (in blue) phases of MgO obtained with DFPT (lines) and TDEP (filled circles) at 7.75 g/cm^3 . Inset: difference between the free energies of the B1 and the B2 phases in QHA (solid line) and with the TDEP method (filled circles and dotted line)

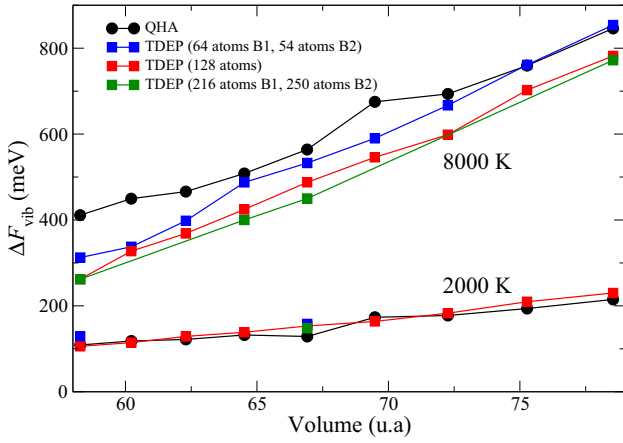


FIG. 4. Vibrational free-energy differences between the B1 and B2 phases at 2000 and 8000 K for the QHA (black circles) and with the TDEP method as a function of the supercell size.

At 8000 K we observe a size effect. The smaller supercell sizes overestimate the free-energy differences, favoring the B2 phase, while the calculations with 128 atoms and more are in agreement. We also observe a larger difference between TDEP and QHA for smaller volumes (larger pressure). This seems in contradiction with the belief that anharmonic effects should decrease with pressure along an isotherm. In fact, it is not. For both phases, the difference between QHA and TDEP decreases with the volume, but not in the same ratio: F_{vib} of the B2 phase becomes closer to the QHA value than for the B1 phase.

Our results for the phase transition boundary are presented in Fig. 5 in comparison with the previous theoretical data of Fig. 1. First, our QHA results are in agreement with the work of Belonoshko *et al.* [9] and Cebulla *et al.* [11] with similar slopes of phase boundary (see the inset of Fig. 5). We therefore observe the same discrepancy with the QHA data of Root *et al.* [12]. The phase boundary predicted with the TDEP method is steeper, increasing the stability domain of the B1 phase at high temperature. Consequently, our curve

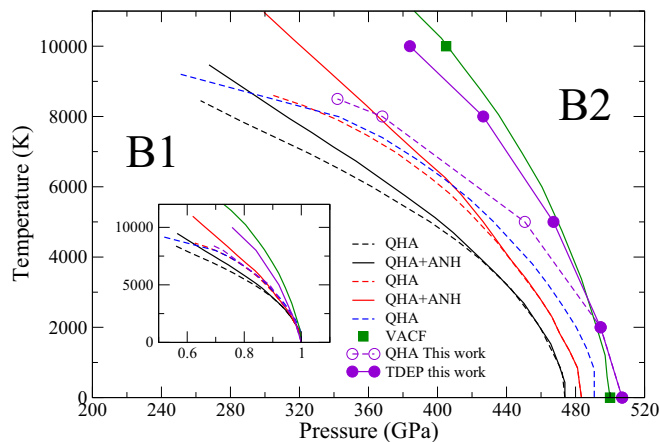


FIG. 5. Same as Fig. 1, with our QHA results (purple open circles and dotted line) and TDEP results (purple filled circles and solid line).

is in agreement with the one obtained by Boates *et al.* [10] using the velocity autocorrelation functions (VACF) method and which, in principle, should take into account the full anharmonicity of the simulated system. The previous attempts to go beyond the QHA [11,12] and to include the intrinsic anharmonicity predicted also an extension of the stability domain of the B1 phase, but to a lesser extent than the one that we obtain with the TDEP. In the next section we analyze these discrepancies and we will try to reconcile, if possible, the different methods.

B. Comparison with previous calculations

Cebulla *et al.* [11] propose to take into account the anharmonicity by expressing the internal anharmonic energy U_{anh} with

$$U_{\text{anh}} = U_{\text{AIMD}} + E_{\text{KIN}} - U_{\text{vib}} - E_0, \quad (4)$$

where U_{AIMD} and E_{KIN} are, respectively, the internal and kinetic energies of the AIMD, E_0 the electronic ground-state energy, and U_{vib} is the harmonic internal energy given by

$$U_{\text{vib}}(V, T) = \int_0^\infty d\omega g(\omega(V, T)) \hbar\omega(T)/2 \coth(\hbar\omega(V, T)/2k_B T). \quad (5)$$

Then, the anharmonic free energy at a temperature T_f is obtained via a thermodynamic integration from an initial temperature T_i :

$$F_{\text{anh}}(T_f) = F_{\text{anh}}(T_i) \frac{T_f}{T_i} - T_f \int_{T_i}^{T_f} \frac{U_{\text{anh}}(T)}{T^2} dT. \quad (6)$$

Since $F_{\text{anh}}(T_i)$ is not known, the idea is to infer a temperature where this energy is negligible and to eliminate the first term of the right-hand side of Eq. (6). This temperature has also to be high enough to neglect the zero-point motion energy contained in U_{vib} but not taken into account in U_{AIMD} since the atomic motions follow a classical trajectory. In the same way, the temperature should be high enough so that the kinetic part contained in U_{vib} reaches the classical value of $3k_B T$ given by the AIMD. Cebulla *et al.* [11] chose a value of $T_i = 3000$ K. At this temperature and above, since the QHA and the TDEP are based on the harmonic approximation, U_{vib} will be equal in both models to the classical value of $3k_B T$ and, obviously, Eq. (6) will give the same correction. In other terms, this method is completely independent of the shape of the PDOS (see Fig. 2). So, it clearly neglects the fact that the phonon frequencies are temperature dependent and it will not correct F_{vib} : this intrinsic anharmonicity will still be missing in F_{anh} . Therefore, the QHA and the TDEP cannot be reconciled with this method. But, it can be used to estimate the anharmonic part not included in the TDEP.

To avoid the problem of the zero-point motion and the kinetic energy we can use the harmonic potential energy [35] directly calculated with the IFCs obtained with the TDEP to calculate the anharmonic internal energy:

$$U_{\text{anh}} = U_{\text{AIMD}} - 1/2 \sum_{ij} \Phi_{ij} u_i u_j - E_0, \quad (7)$$

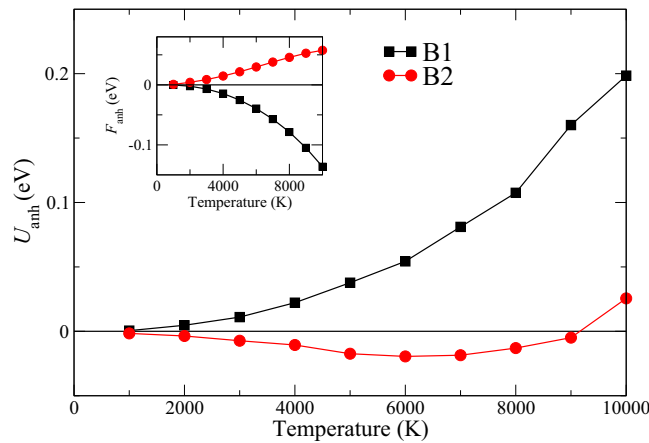


FIG. 6. Internal anharmonic energy U_{anh} for the B1 (in black) and B2 (in red) phases as a function of temperature obtained with Eq. (7) at 6.75 g/cm^3 . Inset: F_{anh} as a function of temperature.

where the Φ_{ij} are the IFCs and u_i the atomic displacements. We present in Fig. 6 the internal anharmonic energy as a function of temperature and for a density of 6.75 g/cm^3 . At low temperature U_{anh} converges toward zero, the atomic motions in both phases are purely harmonic. As the temperature increases, anharmonic effects arise and strongly depend of the structure. For the B2 phase, U_{anh} is negative and close to zero, while it strongly increases with temperature for the B1 phase. This shows again that anharmonic effects are more important in the B1 phase than in the B2 one and that even at high pressure, these effects cannot be neglected. Following Eq. (6), we can calculate F_{anh} (see the inset of Fig. 6). Compared to the QHA, the intrinsic anharmonic effects described by the TDEP lower the vibrational free-energy difference between the B1 and B2 phases (see Fig. 3), pushing the phase boundary to higher pressure at high temperature. If we add F_{anh} to F_{vib} obtained with TDEP, it will have a cumulative effect and the phase boundary will steepen even further. For the B1 phase, F_{anh} counts for about 20% of the anharmonic correction to the QHA, the rest being given by the TDEP, while for the B2 phase, F_{anh} is positive, so slightly brings back the TDEP toward the QHA value by 5%.

Root *et al.* [12] propose another approach to go beyond the QHA based on a thermodynamic integration (TI) to calculate the change in entropy along an isochore:

$$\Delta S = \int_{T_i}^{T_f} \frac{1}{T} \left(\frac{\partial U_{\text{AIMD}}}{\partial T} \right)_V dT. \quad (8)$$

The main drawback of this method is obviously the number of simulations required to obtain the entropy at high temperature. The authors used an increment of 250 K, which means that to have the entropy at 8000 K, starting from 1000 K, about 30 AIMD simulations are necessary. Multiplied by the number of isochores, the computational cost can rapidly become too cumbersome.

We have compared this method with the TDEP one on several isochores, using the same supercell sizes as in Ref. [12], 64 and 54 atoms in the B1 and B2 phases, respectively. An example of the entropy differences between the two phases is given in Fig. 7 for $\rho = 7.75 \text{ g/cm}^3$. In QHA this difference

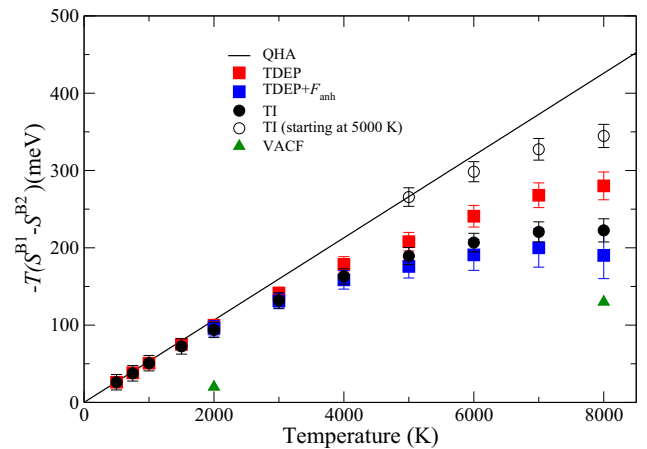


FIG. 7. Entropy difference between the B1 and B2 phases at 7.75 g/cm^3 as a function of the temperature. The solid line corresponds to the QHA, the filled black circles to the TI of Eq. (8), and the red squares to TDEP. The blue squares are similar to the red ones with the correction F_{anh} of Eq. (6), while the open black circles correspond to a TI starting at 5000 K. The green triangles are the results of the VACF at 2000 and 8000 K. The error bars have been estimated with respect to calculation with supercell sizes of 216 atoms and 250 atoms for the B1 and the B2 structures, respectively.

is a straight line, proportional to the temperature. Note that we have neglected the zero-point motion and other quantum effects not included in Eq. (8), but they have a small impact and only at low temperatures. The agreement between TDEP, Eq. (8), and QHA is excellent up to 2000 K where we start to observe a deviation. As the temperature increases, the entropy difference between B1 and B2 diminishes compared to the QHA, as already shown in Fig. 3. The effect is stronger with Eq. (8) than with TDEP, meaning that it will push the phase boundary to higher pressures than the ones obtained with TDEP, a result in contradiction with the lower pressures reported by Root *et al.* [12] (see Fig. 5).

To understand these discrepancies, we have first checked the influence of the exchange correlation functional since Root *et al.* [12] use the Armiento-Mattson (AM05) [19] while we use the LDA. The vibrational free energies obtained with TDEP are slightly different (few meV), but in favor of the B1 phase with AM05 compared to LDA. Therefore, the discrepancies that we observe compared to Ref. [12] can not be attributed to the choice of the exchange correlation functional. Root *et al.* [12] mentioned deviation with the QHA around 5000 K and 400 GPa, while we already observed an effect at 2000 K. If we use this value of 5000 K as the starting temperature for the TI, we underestimate the entropy differences, as shown by the open circles in Fig. 7. The consequence is of course a phase transition at pressures closer to the ones predicted by QHA and therefore by Root *et al.* [12]. We have also performed calculations with bigger supercells, 128 and 216 atoms for the B1 phase, 128 and 250 atoms for the B2 phase. At 2000 K the internal energy is converged to 1 meV as a function of the supercell size, but at 8000 K we observe differences up to 5 meV. This supercell size effect is similar to the one that we observe for the TDEP method (see Fig. 4),

where we have shown that a small supercell favors the B2 phase.

Since Eq. (8) is based on the internal energy coming from AIMD simulations with no further approximation as in TDEP, it should in principle contain the whole anharmonicity of the simulated system. The difference that we observe between TI and TDEP is close to F_{anh} obtained with the method of Cebulla *et al.* [11] and if we add this correction to the entropy found in TDEP, we almost recover the TI (see Fig. 7). This confirms that the anharmonic terms that we do not take into account with TDEP correct to a larger extent the QHA.

Boates *et al.* [10] used the Fourier transforms of the velocity autocorrelation functions (VACF) to calculate the vibrational entropies. They obtained a transition pressure of 405 GPa at 10 000 K, close to the value obtained with the TDEP method (see Fig. 5). This method is usually used with classical MD since it requires large supercells and considerably long simulation time to obtain the PDOS. Boates *et al.* [10] used 64 and 128 atoms only in their supercells for the B1 and B2 phases, respectively. We have performed simulations up to 20 ps for several ρ , T points to obtain the VACF and to calculate the vibrational free energies. This led us to think that the supercell sizes used in Ref. [10] are not large enough to converge the free energy. At 2000 K and 7.75 g/cm^3 , for example, a temperature where anharmonicity should be negligible, we do not recover the QHA result, due to a strong underestimation of the vibrational free energy of the B1 phase (100 meV), partially compensated by a similar effect on the B2 phase (40 meV) (see Fig. 7). At 8000 K, it is slightly better, but again, certainly due to a cancellation of errors between the two phases.

To sum up, we are now able to explain the discrepancies between our calculations and the previous ones. These differences come from the treatment of the intrinsic anharmonic part for Cebulla *et al.* [11] or by an overestimation of the temperature at which the anharmonic effects have to be taken into account for Root *et al.* [12]. Concerning the work of Boates *et al.* [10], we do not recover their results.

C. Comparison with experiments

Figure 8 shows the experimental P - T curves with our calculated B1-B2 transition line and Hugoniot. We plot also recent *ab initio* predictions of the melting curve [9,12]. Recently, two decaying shock experiments [14,15] have studied the phase diagram of MgO. In the first one [14], a clear bump and a slight slope change were observed in the P - T curve along the Hugoniot. The strong bump at 450 GPa was interpreted as the B1-B2 phase transition and the second one at 650 GPa, much softer, as the B2 melt. The second experiment [15] reported only the first bump, at similar thermodynamic conditions, but did not observe the slope change at higher pressure. Contrary to Ref. [14], they interpreted this feature as the B2 melt and not the B1-B2 solid phase transition, similarly to interpretation of decaying shock experiments performed on SiO₂ [50] or MgSiO₃ [51]. In addition, with impact shock compression experiments, Root *et al.* [12] observed only one break in the Hugoniot around 360 GPa. Note that if a bump along the Hugoniot can be attributed to a phase transition, the nature of this phase transition cannot be determined in the

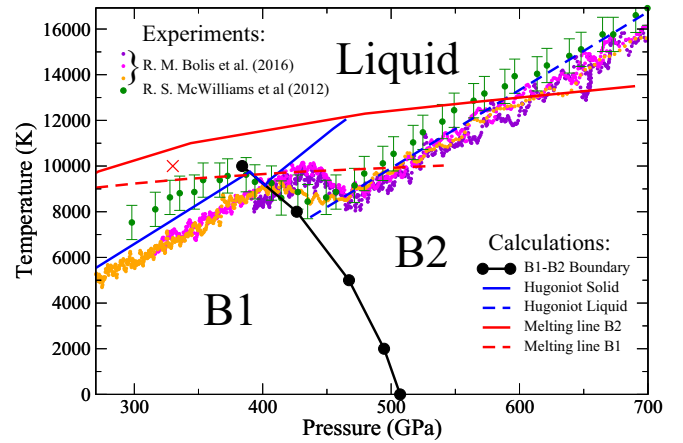


FIG. 8. Experimental shock temperature data in comparison with our predicted B1-B2 phase boundary. Purple, magenta, and orange dots: Bolis *et al.* [15]; green dots: McWilliams *et al.* [14]. The black solid line with filled circles is the B1-B2 boundary obtained with TDEP and the blue line the calculated Hugoniot. The dashed blue line is an extension of our Hugoniot curve for the liquid phase in the stability domain of the solid phase. The red curve is the calculated melt line of Root *et al.* [12] for the B2 structures and the red dashed one is the calculated melt line of de Koker *et al.* [53] for the B1 structure. The red cross indicates the melting of an AIMD with B2 as the starting structure of the simulation.

absence of microscopic *in situ* diagnostics. Can our calculations help to solve this controversy?

Our predicted B1-B2 phase boundary is close to the bump observed in the decaying shock experiments at 450 GPa. Knowing that anharmonic effects not included in our calculations should increase the stability domain of the B1 phase (see the discussion in the previous section), a nice correlation between the bump observed in decaying shock and the B1-B2 phase transition could be deduced. However, different arguments are on the side of a melting observation during decaying shock experiments. First, the low intensity or absence of a second bump related to melting signature in McWilliams *et al.* [14] is ambiguous, as a large thermodynamic domain is investigated (up to 1 TPa and 30 000 K) far above the predicted melting line [9,10,12,16,52]. Second, there is a strong disagreement between the calculated Hugoniot for the B2 phase and the experimental points above 450 GPa, as already noted by Cebulla *et al.* [11]. The theoretical Hugoniot in the B1 domain is consistent with the lower part of the experimental results (below 450 GPa). After the bump, the experimental points are close to our calculated liquid Hugoniot. This comparison between our theoretical and experimental Hugoniots seems therefore to indicate a direct transition between the B1 and the liquid phase along the Hugoniot, close to the triple point, with a melting point around 450 GPa and 10 000 K as proposed in Ref. [15]. This melting point is close to the computed melting line of the B1 phase of de Koker *et al.* [53], using a comparison of the Gibbs free energies of the solid and the liquid and based on AIMD, but also with extrapolation of the B1 melting line obtained with the Z method by Belonoshko *et al.* [9,54] and with the two phase calculations of Root *et al.* [12] and Musella *et al.* [55]. But

in this region, the calculated melting line of the B2 phase is above the results for the B1 phase [12] (see Fig. 8).

Ab initio calculations of melting curves are difficult and their uncertainties can be around several hundred kelvin. These uncertainties are cumulative when comparing melting lines obtained with different structures. In our simulations, at 6.0 g/cm³ and 10 000 K, corresponding to a pressure of 330 GPa, the B2 structure melts spontaneously (see the red cross on Fig. 8), contrary to the B1 structure, while at the same density and 9000 K (283 GPa), the B2 structure stays solid. This melting of the perfect crystal along an isochore is known as the *heat until it melts* method and generally induces a superheating that results in an overestimation of the melting temperature [56]. New simulations, with larger supercells and with new methods to determine the melting, are necessary to clarify this debate. In parallel, shock or diamond anvil cells experiments, coupled with x-ray diffraction, are strongly needed.

IV. THERMODYNAMICS PROPERTIES

One of the main advantages of using the TDEP method is that we can not only calculate a temperature-dependent free energy, but also extract from the AIMD various thermodynamical quantities as the thermoelasticity, the Grüneisen parameters, or the thermal expansion.

A. Thermoelasticity

The elastic constants can be obtained from the second-order force constants following [57–59]:

$$C_{\alpha\beta\gamma\delta} = A_{\alpha\gamma\beta\delta} + A_{\beta\gamma\alpha\delta} - A_{\alpha\beta\gamma\delta} \quad (9)$$

with

$$A_{\alpha\beta\gamma\delta} = \frac{1}{2V} \sum_{ij} \Phi_{ij}^{\alpha\beta} d_{ij}^{\gamma} d_{ij}^{\delta}, \quad (10)$$

where d_{ij}^{α} is the α th component of the distance between the atoms i and j . The full elastic constants matrix $C_{\alpha\beta\gamma\delta}$ can be reduced following the symmetries and the Voigt notation. The temperature effects are then directly introduced in the elastic constants by the temperature variation of the IFCs. As shown by Shulumba *et al.* [59], this method is much faster and practical than the one using deformation matrix which needs several AIMD simulations or based on the QHA to calculate the free energies from the phonon dispersions of the strained lattices [60]. The main drawback of this method is that since the elastic constants are related to phonon frequencies in the long-wavelength limit, it requires large supercells to converge the sum in Eq. (10). To circumvent this difficulty, we only retain the temperature dependence of Eq. (10) that we apply to the static calculations at 0 K [59].

We present in Fig. 9 the pressure and temperature evolution of the elastic constants (C_{11} , C_{12} , and C_{44}), the isotropic bulk (K_T), and shear (G) moduli of MgO for the B1 and B2 phases, calculated using the TDEP method. K_T and G were obtained using the Voigt-Reuss-Hill average. For our 0-K results, we use the stress-strain relations and a deformation matrix applied on the cubic unit cell of the B1 and B2 phases. We also plot on Fig. 9 the results of Karki *et al.* [60,61] at

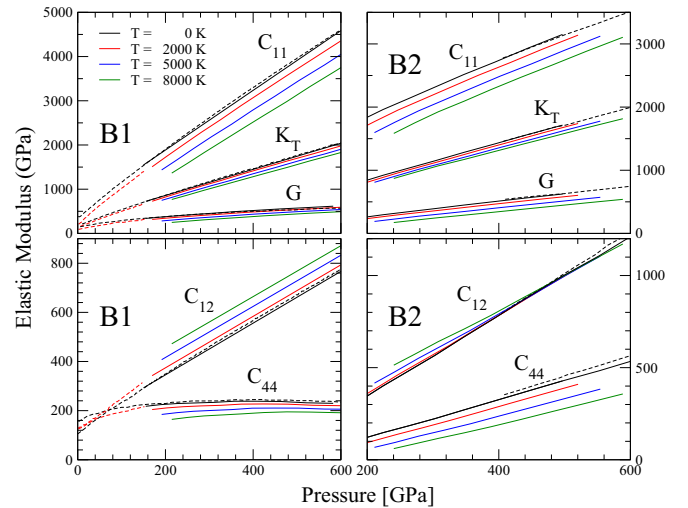


FIG. 9. Elastic constants C_{11} , C_{12} , and C_{44} , isotropic bulk (K_T), and shear (G) moduli of MgO of the B1 and B2 phases as a function of pressure and temperature. The dashed lines are the results of Karki *et al.* [60,61] at 0 K (black) and at 2000 K (red) using the QHA.

0 K and at 2000 K using the QHA (for the B1 phase). For both phases we observe a softening of C_{11} and C_{44} while C_{12} hardens with temperature. For the B1 phase, C_{44} shows almost no pressure dependence above 150 GPa and the effect of the temperature is also very weak. In the B2 phase, C_{44} has a different behavior: it increases with pressure and softens with temperature. Since K_T is given by $(C_{11} + 2C_{12})/3$, the effect of temperature on these two elastic constants cancel each other to result in a small decrease of the bulk modulus in temperature for both phases. The shear modulus G evolves in temperature in a similar way than C_{44} .

B. Grüneisen parameter

The Grüneisen parameter γ provides a bridge between P and T and is a key quantity for the Earth's interior where P as a function of depth is well constrained, thanks to seismological data, but T is still poorly known. The evolution of γ with density, but also with temperature, is therefore essential to build reliable EOS for planetary modeling [62,63]. The mode Grüneisen parameters are defined by the volume derivatives of the phonon-mode frequencies:

$$\gamma_s = -\frac{V}{\omega_s} \left(\frac{\partial \omega_s}{\partial V} \right)_T. \quad (11)$$

They can be obtained from the third-order force constants Ψ_{ijk} following [40]:

$$\gamma_s(\mathbf{q}) = -\frac{1}{6\omega_s^2(\mathbf{q})} \sum_{ijk\alpha\beta\gamma} \Psi_{ijk}^{\alpha\beta\gamma} \frac{X_{is}^{\alpha}(\mathbf{q})X_{js}^{\beta}(\mathbf{q})}{\sqrt{M_i M_j}} r_k^{\gamma} \exp[i\mathbf{q}\cdot\mathbf{R}_j], \quad (12)$$

where M_i and r_i^{α} are the mass and the α th component of the vector position of atom i , ω_s the frequency of mode s , the X 's are the eigenvectors, and \mathbf{R}_i the lattice vector of the unit cell of atom i .

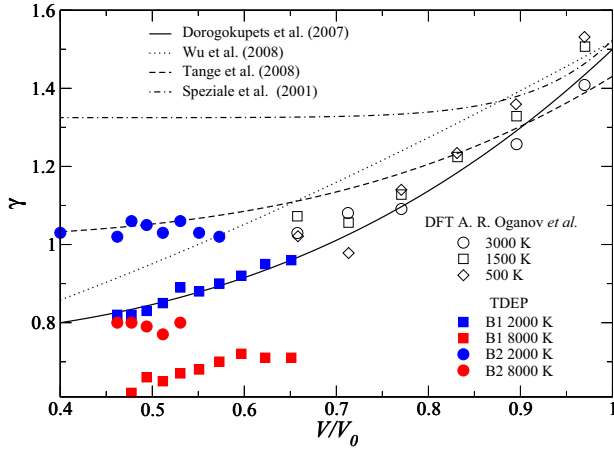


FIG. 10. Grüneisen parameter of MgO. The black open symbols are the effective Grüneisen parameter of Oganov *et al.* [69]. The lines are Grüneisen parameters used in semiempirical equation of state [8,65,66,68].

From the γ_s 's the thermodynamical Grüneisen parameter is obtained by

$$\gamma = \frac{\sum_{s=1}^{3N_a} \gamma_s C_{V,s}}{C_V}, \quad (13)$$

where the $C_{V,s}$ are the mode heat capacities, and C_V the specific heat.

In EOS, a commonly used expression for the volume dependence of the Grüneisen parameter has been given by Al'tshuler *et al.* [64]:

$$\gamma = \gamma_\infty + (\gamma_0 - \gamma_\infty)x^\beta, \quad (14)$$

where γ_0 is the Grüneisen parameter at ambient conditions, γ_∞ is the Grüneisen parameter at infinite compression ($x = V/V_0 = 0$), and β is a fitted parameter. Since MgO has a long history as an internal pressure standard at extremely high pressure and temperature there are a large collection of parameters for the volume dependence of its Grüneisen parameter. The Mie-Grüneisen model has been used to reproduce experimental P - V - T data and obtain the parameters entering Eq. (14).

We present in Fig. 10 several versions of Eq. (14) based on experimental data [8,65–68] and the results of Oganov *et al.* [69] based on theoretical P - V - T points obtained with AIMD, while the corresponding fitting parameters are given in Table I. We also report our values obtained with Eq. (13) for

TABLE I. Fitting parameters of function 14 of the Grüneisen parameter of the B1 phase of MgO.

EOS	γ_0	γ_∞	β
This work	1.440	0.800	3.255
PAW [69]	1.455	0.841	3.057
Dorogokupets <i>et al.</i> [66]	1.50	0.75	2.96
Wu <i>et al.</i> [8]	1.520	0.606	1.406
Tange <i>et al.</i> [68]	1.431	1.016	3.50
Speziale <i>et al.</i> [65]	1.524	1.325	11.8

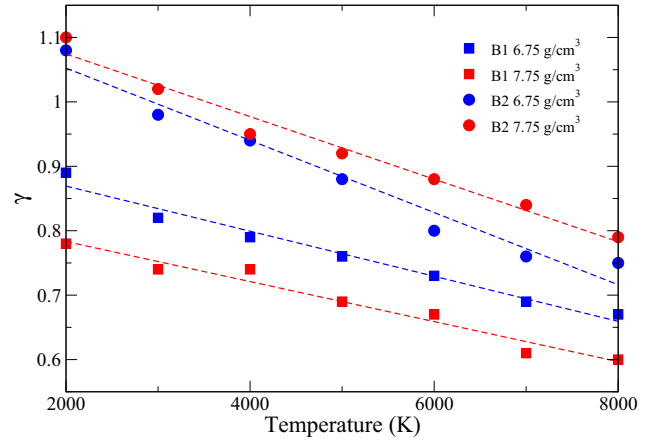


FIG. 11. Temperature dependence of the Grüneisen parameter of MgO for the B1 (squares) and B2 (circles) phases at 6.25 g/cm³ (red) and 7.75 g/cm³ (blue). The dashed lines are linear fits of these data.

the B1 and B2 phases at 2000 and 8000 K. We have performed an AIMD at 300 K and at the equilibrium volume of the B1 phase. We obtain a value of 1.44 for the Grüneisen parameter, close to the experimental value of 1.54. Using this value as γ_0 we have fitted our results for the B1 phase at 2000 K to obtain γ_∞ and β (see Table I). Our direct calculations of γ are close to the results of Oganov *et al.* [69] obtained by fitting the thermal pressure extracted of AIMD simulations performed with GGA. Our results are also in good agreement with the semiempirical EOS proposed by Dorogokupets *et al.* [66]. For the B2 phase we find larger values for γ , about 25%, compared to the B1 phase. We observe a similar difference in the thermal pressure extracted from AIMD simulations. For the B2 phase, the volume dependence of γ is rather weak. We performed an AIMD simulation at 9 g/cm³ ($V/V_0 = 0.4$) and we obtain a value of 1.08.

In the Mie-Grüneisen EOS, the temperature dependence of γ at constant V is neglected to directly obtain the thermal pressure in terms of the thermal energy: $P_{TH} = \gamma E_{TH}/V$. Anderson [62] has shown that this assumption does not hold for MgO. Using experimental data, he obtained, at constant V , a value of 1.39 at 1800 K, so 10% lower than at room temperature. At 8000 K, and for larger compression, we also observed a decrease of γ with temperature (see Figs. 10 and 11). The effect is larger for the B1 phase and is almost constant with volume, while for the B2 phase the temperature dependence diminishes with the compression (Fig. 11). This shows the limitation of the Mie-Grüneisen approach to obtain the thermal pressure.

C. Wave velocities

From the Grüneisen parameter we can also obtain the volume thermal expansion coefficient defined as

$$\alpha_V = \frac{\gamma C_V}{K_T V}. \quad (15)$$

Then, knowing γ and α , we can obtain the adiabatic incompressibility $K_S = (1 + \alpha\gamma T)K_T$ and with the shear modulus

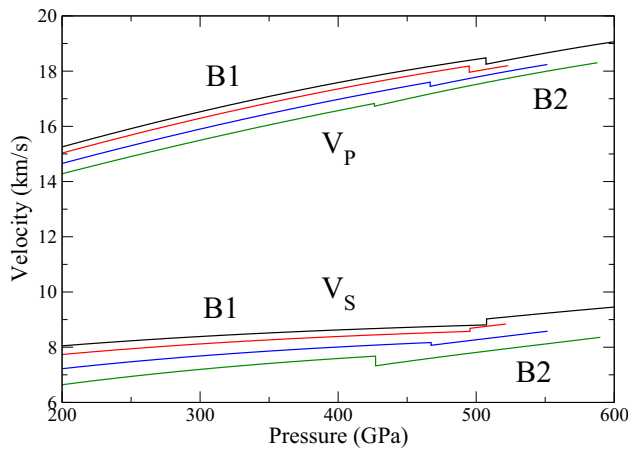


FIG. 12. Compressional and shear wave velocities of MgO as a function of pressure at 0 (black), 2000 (red), 5000 (blue), and 8000 K (green). The kink in the curves indicates the phase transition between B1 and B2.

G , the compressional and shear wave velocities V_p and V_s following:

$$V_p = \sqrt{\frac{K_S + 4/3G}{\rho}}, \quad (16)$$

$$V_s = \sqrt{\frac{G}{\rho}}. \quad (17)$$

Our results are presented in Fig. 12. In both phases, V_p has a similar pressure and temperature dependence while V_s shows a larger pressure and temperature dependence in the B2 phase that are mainly due to the differences observed in the evolution of the elastic constant C_{44} between B1 and B2 (see

Fig. 9). Compared to iron, temperature has a weaker effect on the wave velocities. Martorell *et al.* [70] predict a decrease of 8.6% and 29.6% for V_p and V_s in iron at 6000 K (before the premelting effect [71]) and 360 GPa while we found 4.5% and 9.7% for the same conditions.

V. CONCLUSIONS

Using a recent method to calculate the vibrational contribution to the free energy we have studied the phase transition between the B1 and B2 phases in MgO. Compared to previous theoretical works, we obtain a stronger correction to the quasiharmonic approximation at high temperature which pushes the transition line to higher pressures. We show that anharmonic effects cannot be neglected and have to be carefully calculated. We have also estimated the anharmonic part not described by our method and we show that its effect is to further increase the transition pressure. Superimposed on recent shock experiments, our results indicate a direct transition between the B1 structure toward the liquid along the Hugoniot close to the triple point B1-B2 liquid. New experiments using x-ray diffraction are necessary to confirm this assertion. Using the full capabilities of the TDEP, we also derive several thermodynamic quantities as the elastic constants, the Grüneisen parameters, and the sound velocities that are crucial quantities to build reliable high-pressure high-temperature EOS to describe planetary interiors.

ACKNOWLEDGMENTS

We would like to thank X. Gonze for helpful discussions. We also thank M. Desjarlais for sharing with us details of the method used in Ref. [12]. This research was supported by the ANR Grant No. PLANETLAB 12-BS04-0015.

-
- [1] D. Valencia, R. J. O'Connell, and D. Sasselov, *Icarus* **181**, 545 (2006).
- [2] T. Guillot, *Annu. Rev. Earth Planet. Sci.* **33**, 493 (2005).
- [3] H. F. Wilson and B. Militzer, *Phys. Rev. Lett* **108**, 111101 (2012).
- [4] M. J. Mehl, R. E. Cohen, and H. Krakauer, *J. Geophys. Res.* **93**, 8009 (1988).
- [5] A. Strachan, T. Çağın, and W. A. Goddard, *Phys. Rev. B* **60**, 15084 (1999).
- [6] A. R. Oganov, M. J. Gillan, and G. D. Price, *J. Chem. Phys.* **118**, 10174 (2003).
- [7] D. Alfè, *Phys. Rev. Lett* **94**, 235701 (2005).
- [8] Z. Wu, R. M. Wentzcovitch, K. Umemoto, B. Li, K. Hirose, and J.-C. Zheng, *J. Geophys. Res.* **113**, B06204 (2008).
- [9] A. B. Belonoshko, S. Arapan, R. Martonak, and A. Rosengren, *Phys. Rev. B* **81**, 054110 (2010).
- [10] B. Boates and S. A. Bonev, *Phys. Rev. Lett* **110**, 135504 (2013).
- [11] D. Cebulla and R. Redmer, *Phys. Rev. B* **89**, 134107 (2014).
- [12] S. Root, L. Shulenburger, R. W. Lemke, D. H. Dolan, T. R. Mattsson, and M. P. Desjarlais, *Phys. Rev. Lett* **115**, 198501 (2015).
- [13] F. Coppari, R. F. Smith, J. H. Eggert, J. Wang, J. R. Rygg, A. Lazicki, J. A. Hawreliak, G. W. Collins, and T. S. Duffy, *Nat. Geosci.* **6**, 926 (2013).
- [14] R. S. McWilliams, D. Spaulding, J. H. Eggert, P. Celliers, D. G. Hicks, R. F. Smith, G. W. Collins, and R. Jeanloz, *Science* **338**, 1330 (2012).
- [15] R. M. Bolis, G. Morard, T. Vinci, A. Ravasio, E. Bambrink, M. Guarguaglini, M. Koenig, R. Musella, F. Remus, J. Bouchet, N. Ozaki, K. Miyanashi, T. Sekine, Y. Sakawa, T. Sano, R. Kodama, F. Guyot, and A. Benuzzi-Mounaix, *Geophys. Res. Lett.* **43**, 9475 (2016).
- [16] K. Miyanishi, Y. Tange, N. Ozaki, T. Kimura, T. Sano, Y. Sakawa, T. Tsuchiya, and R. Kodama, *Phys. Rev. E* **92**, 023103 (2015).
- [17] D. M. Ceperley and B. J. Alder, *Phys. Rev. Lett.* **45**, 566 (1980).
- [18] J. P. Perdew, K. Burke, and M. Ernzerhof, *Phys. Rev. Lett* **77**, 3865 (1996).
- [19] R. Armiento and A. E. Mattsson, *Phys. Rev. B* **72**, 085108 (2005).
- [20] X. Gonze, *Phys. Rev. B* **55**, 10337 (1997).
- [21] X. Gonze and C. Lee, *Phys. Rev. B* **55**, 10355 (1997).

- [22] S. Baroni, S. de Gironcoli, A. D. Corso, and P. Gianozzi, *Rev. Mod. Phys.* **73**, 515 (2001).
- [23] K. Parlinski, J. Łażewski, and Y. Kawazoe, *J. Phys. Chem. Solids* **61**, 87 (2000).
- [24] B. Fultz, *Prog. Mater. Sci.* **55**, 247 (2010).
- [25] P. Souvatzis, O. Eriksson, M. I. Katsnelson, and S. P. Rudin, *Phys. Rev. Lett* **100**, 095901 (2008).
- [26] O. Hellman, I. A. Abrikosov, and S. I. Simak, *Phys. Rev. B* **84**, 180301(R) (2011).
- [27] J. Bouchet and F. Bottin, *Phys. Rev. B* **95**, 054113 (2017).
- [28] B. Dorado, F. Bottin, and J. Bouchet, *Phys. Rev. B* **95**, 104303 (2017).
- [29] A. Glensk, B. Grabowski, T. Hickel, and J. Neugebauer, *Phys. Rev. Lett* **114**, 195901 (2015).
- [30] B. Grabowski, L. Ismer, T. Hickel, and J. Neugebauer, *Phys. Rev. B* **79**, 134106 (2009).
- [31] A. Erba, M. Shahrokhi, R. Moradian, and R. Dovesi, *J. Chem. Phys.* **142**, 044114 (2015).
- [32] Z. Wu and R. M. Wentzcovitch, *Phys. Rev. B* **79**, 104304 (2009).
- [33] I. Errea, M. Calandra, and F. Mauri, *Phys. Rev. Lett* **111**, 177002 (2013).
- [34] I. Errea, M. Calandra, and F. Mauri, *Phys. Rev. B* **89**, 064302 (2014).
- [35] O. Hellman, P. Steneteg, I. A. Abrikosov, and S. I. Simak, *Phys. Rev. B* **87**, 104111 (2013).
- [36] J. Bouchet and F. Bottin, *Phys. Rev. B* **92**, 174108 (2015).
- [37] T. Tadano, Y. Gohda, and S. Tsuneyuki, *J. Phys.: Condens. Matter* **26**, 225402 (2014).
- [38] L. J. Nelson, G. L. W. Hart, F. Zhou, and V. Ozolinš, *Phys. Rev. B* **87**, 035125 (2013).
- [39] K. Esfarjani and H. T. Stokes, *Phys. Rev. B* **77**, 144112 (2008).
- [40] O. Hellman and I. A. Abrikosov, *Phys. Rev. B* **88**, 144301 (2013).
- [41] The ABINIT code is a common project of the Catholic University of Louvain (Belgium), Corning Incorporated, CEA (France), and other collaborators, <http://www.abinit.org>.
- [42] X. Gonze, B. Amadon, P.-M. Anglade, J.-M. Beuken, F. Bottin, P. Boulanger, F. Bruneval, D. Caliste, R. Caracas, M. Côté, T. Deutsch, L. Genovese, P. Ghosez, M. Giantomassi, S. Goedecker, D. Hamann, P. Hermet, F. Jollet, G. Jomard, S. Leroux *et al.*, *Comput. Phys. Commun.* **180**, 2582 (2009).
- [43] D. J. Hooton, *Z. Phys.* **142**, 42 (1955).
- [44] A. Dewaele, V. Stutzmann, J. Bouchet, F. Bottin, F. Occelli, and M. Mezouar, *Phys. Rev. B* **91**, 134108 (2015).
- [45] P. E. Blöchl, *Phys. Rev. B* **50**, 17953 (1994).
- [46] M. Torrent, F. Jollet, F. Bottin, G. Zerah, and X. Gonze, *Comput. Mater. Sci.* **42**, 337 (2008).
- [47] N. Holzwarth, A. Tackett, and G. Matthews, *Comput. Phys. Commun.* **135**, 329 (2001).
- [48] ATOMPAAW is a general license public code developed at Wake Forest University. Some of its capabilities have been developed at the Commissariat à l'énergie atomique, <http://pwpaw.wfu.edu>.
- [49] A. Dewaele, M. Torrent, P. Loubeyre, and M. Mezouar, *Phys. Rev. B* **78**, 104102 (2008).
- [50] M. Millot, N. Dubrovinskaia, S. B. A. Černok, L. Dubrovinsky, D. G. Braun, P. M. Celliers, G. W. Collins, J. H. Eggert, and R. Jeanloz, *Science* **347**, 418 (2015).
- [51] D. E. Fratanduono, M. Millot, R. G. Kraus, D. K. Spaulding, G. W. Collins, P. M. Celliers, and J. H. Eggert, *Phys. Rev. B* **97**, 214105 (2018).
- [52] T. Taniuchi and T. Tsuchiya, *J. Phys.: Condens. Matter* **30**, 114003 (2018).
- [53] N. de Koker and L. Stixrude, *Geophys. J. Int.* **178**, 162 (2009).
- [54] A. B. Belonoshko, S. Davis, N. V. Skorodumova, P. H. Lundow, A. Rosengren, and B. Johansson, *Phys. Rev. B* **76**, 064121 (2007).
- [55] R. Musella, S. Mazevet, and F. Guyot, *Phys. Rev. B* **99**, 064110 (2019).
- [56] J. Bouchet, F. Bottin, G. Jomard, and G. Zerah, *Phys. Rev. B* **80**, 094102 (2009).
- [57] G. Liebfried and W. Ludwig, *Solid State Physics* (Academic, New York, 1961).
- [58] D. C. Wallace, in *Thermodynamics of Crystals*, edited by P. Ziesche and H. Eschrig (Wiley, New York, 1972).
- [59] N. Shulumba, O. Hellman, L. Rogström, Z. Raza, F. Tasnádi, I. A. Abrikosov, and M. Odén, *Appl. Phys. Lett.* **107**, 231901 (2015).
- [60] B. B. Karki, R. M. Wentzcovitch, S. de Gironcoli, and S. Baroni, *Science* **286**, 1705 (1999).
- [61] B. B. Karki, *Phys. Earth Planet. Inter.* **240**, 43 (2015).
- [62] O. L. Anderson, *Geophys. J. Int.* **143**, 279 (2000).
- [63] F. D. Stacey, *Rep. Prog. Phys.* **68**, 341 (2005).
- [64] L. V. Al'tshuler, S. E. Brusnikin, and E. A. Kuz'menkov, *J. Appl. Mech. Tech. Phys.* **28**, 129 (1987).
- [65] S. Speziale, C. Zha, T. S. Duffy, R. J. Hemley, and H. K. Mao, *J. Geophys. Res.* **106**, 515 (2001).
- [66] P. I. Dorogokupets and A. Dewaele, *High Pressure Res.* **27**, 431 (2007).
- [67] P. I. Dorogokupets, *Phys. Chem. Miner.* **37**, 677 (2010).
- [68] Y. Tange, Y. Nishihara, and T. Tsuchiya, *J. Geophys. Res.* **114**, B03208 (2009); **115**, B12203 (2010).
- [69] A. R. Oganov and P. I. Dorogokupets, *Phys. Rev. B* **67**, 224110 (2003).
- [70] B. Martorell, I. G. Wood, J. Brodholt, and L. Vočadlo, *Earth Planet. Sci. Lett.* **451**, 89 (2016).
- [71] B. Martorell, L. Vočadlo, J. Brodholt, and I. G. Wood, *Science* **342**, 466 (2013).